1016 *Macromolecules* **2010**, *43*, 1016–1027
DOI: 10.1021/ma902083z

Macromolecules
ARTICLE

Real-Time X-ray Study of Nylon-6 Fibers during Dehydration: Equatorial Small-Angle Scattering is Due to Surface Refraction

D. T. Grubb*,† and N. S. Murthy‡

†*Department of Materials Science and Engineering, Cornell University, Ithaca, New York 14853 and* ‡*New Jersey Center for Biomaterials, Rutgers University, Piscataway, New Jersey 08854*

Received September 18, 2009; Revised Manuscript Received November 6, 2009

ABSTRACT: The equatorial streak in the small-angle X-ray scattering (SAXS) pattern from nylon-6 fibers, normally assigned to microvoids or to internal fibrillar structure, is due to scattering from the fiber surfaces. This scattering is best thought of as refraction by the cylindrical fibers. The streak intensity increases by 50 times during the early stages of drying a wet bundle of nylon-6 fibers, when superficial water, water between the fibers in the bundle, is lost. Separate X-ray experiments using a nonpenetrating fluid, a large diameter monofilament, and microbeam SAXS confirmed this assignment. There are many fibers where internal voids are known to be the source of a strong equatorial streak in SAXS, but in general, a check for surface scattering is advised before interpreting this feature. Simultaneous small- and wide-angle X-ray diffraction (WAXD) was obtained during drying. Following the initial loss of superficial water, there are changes in both the WAXD reflections and the SAXS lamellar reflection. In the later stages of drying, WAXD shows that the crystals decrease in perfection, in apparent lateral size and in degree of misorientation. Lamellar structure changes are slower to start and include a 1.3% decrease in axial lamellar spacing and a 40% increase in the contrast between the crystalline lamellae and the interlamellar regions. All these changes are explained as effects of the removal of absorbed water from the interlamellar amorphous regions and their reduction in volume and density. Interpretation of these experimental results thus does not require a fibrillar structure in nylon-6.

Introduction

The structure of nylon-6 has been investigated many times using diffraction techniques, and relatively few references will be given here. Wide-angle X-ray diffraction (WAXD) was initially concerned with distinguishing the allomorphs of the polyamides (α and γ for nylon-6) and with measurement of crystallinity. Later, changes in crystalline structure on thermal treatment of fibers,[1] elastic deformation,[2] and plastic deformation[3] were investigated. WAXD also allowed detailed characterization of the amorphous phase in nylon-6 fibers.[4,5]

Most X-ray structural investigations of polymer fibers have used small-angle X-ray scattering (SAXS) or a combination of this and WAXD. The SAXS pattern from nylon-6 fibers is quite typical. It contains a single meridional reflection, called a two point pattern. This may split into a pair of off-axis reflections and is then called a four point pattern. This reflection is taken to come from a repeating structure of crystalline lamellae and interlamellar amorphous regions. On drawing these fibers the spherulitic lamellae reorganize into highly aligned structures, the periodic spacing (long period) changes, and microscopy shows a microfibrillar appearance.[6,7] It is assumed that the lamellar stacks, much longer than they are wide, are the basic unit of this fibrillar microstructure.[8,9] Analysis of the lamellar reflection gives the size of these lamellar stacks,[10,11] and more detailed numerical analysis has been used to give the linear crystallinity of the stack and the size distribution of crystal and amorphous regions in the stack.[12−15]

The observed two-point patterns can be analyzed as unresolved four-point patterns,[16] and the reflections extend neither on a circular arc nor along a layer line perpendicular to the fiber axis, but on an ellipse.[2,17,18] Off-axis reflections imply structures correlated at some angle to the fiber axis, and the standard models for this include lamellae with tilted surfaces and lamellae in adjacent stacks that are correlated in position along the stack. In some cases where the lamellae are wide, tilted surfaces can be seen by microscopy, but that is not the case in nylons. Neither of the standard models gives an easy physical explanation of the observed elliptical trajectory of the reflection.[19]

The SAXS pattern also contains a continuous sharp streak extending out along the equator. This is normally assumed to come from either elongated voids within the fiber or a fibrillar substructure where the lamellar stacks, which contain the crystals, are more dense than the surrounding matrix. It is certainly true that many natural and synthetic fibers, including carbon fibers and most wet-spun fibers, do contain elongated voids. The early assumption was that all such scattering is due to voids.[20] Later it was found that in some cases voids were a minor cause of the scattering[21] or did not fit the data well at all.[22] It is relatively easy to use electron microscopy to find voids, but difficult to prove their absence, so particularly for melt-spun fibers the question of the cause of the equatorial streak is not completely resolved. In the case of nylon-6 TEM has indicated the presence of a fibrillar structure[7,23] and voids are not seen, so most workers have taken fibrils to be the source of the equatorial streak.

The possibility that refraction produces a SAXS signal has been discussed for a long time,[24] and it is understood that refraction and diffraction are limiting cases of the same effect.[25,26] A cylindrical fiber of material with a refractive index less than one (any material at X-ray wavelengths) will act as a divergent lens, spreading the parallel incident beam out. For X-rays the spread is to small angles only, as the refractive index is very close to one. It has been generally assumed that this scattering will be too weak to see in the regular SAXS range, as fibers 20 μm in diameter will

*To whom correspondence should be addressed.

 Published on Web 12/31/2009

have a tiny surface area compared to that of the fibrils, which are ~10 nm in diameter. However, SAXS due to refraction from fibers was observed in 1987,[27] and the refracted signal is now the basis for medical imaging and the NDE of composites.[28−30]

Water has a very significant effect on the processing and properties of polyamides including nylon-6. Changes in microstructure that may underlie these changes in properties are therefore of interest in themselves. At the same time, the water is a probe that can help to determine the structure of the material in more detail. Earlier work on hydration concentrated on the crystallization that occurs when water or other plasticizers are absorbed.[31−33] Many studies of the swelling of stable structures followed. Concentrating on the structure of uniaxially oriented sheet or fiber, the effect of swelling nylon-6 by alcohols and water has been studied by SAXS using paracrystallinity models[34−37] and also using parameters more directly related to the scattering patterns.[16]

X-ray scattering is not the only method used to study hydration in nylon. In 1989, small-angle neutron scattering (SANS) was used in combination with WAXD and SAXS of oriented fibers to study the structural changes on hydration.[38] Later SANS was used to compare hydration in a set of nylon-6 fibers drawn to a range of draw ratios,[39] and in 1998 a detailed SANS study of unoriented nylon-6 and nylon-6,6 used H_2O, D_2O, and partially deuterated ethylene glycol as swelling agents.[40] ^2H NMR,[41−43] IR spectroscopy,[38,44] and dielectric spectroscopy[45] have also been used to study the interaction of water with nylon-6.

It was first thought that water penetrates into the crystals,[46] but later studies showed that the WAXD changes are too slight to be due to included water.[16,38] On the basis of the accepted model for nylon fibers, there are thus three morphologically distinct locations for water: (1) interlamellar, in the amorphous regions within the lamellar stack; (2) interfibrillar, in the amorphous regions between the lamellar stacks; (3) superficial, in voids or on the surface of the fiber.

It might be expected that, as water is of lower density than nylon, access of water to the first two regions would lower the amorphous density and so increase the X-ray scattering contrast between crystalline and amorphous regions. Unfortunately for this simple view, when nylon swells by absorption of water, its density does not change.[16,46] Since the crystals do not absorb water, water is absorbed in the amorphous regions and the volume of amorphous component increases. The volume fraction crystallinity decreases, so the amorphous density must increase to give an approximately constant fiber density. The water interacts strongly with the nylon, breaking hydrogen bonds between chains and lowering T_g so that a new higher density amorphous structure is formed.

Water in the first two regions would thus reduce the density contrast between crystal and amorphous materials and reduce any X-ray scattering intensity. Water in voids or on the surface, region 3 above, will also reduce the density contrast but by a much greater amount. The increase in volume of swollen material matches the uptake of water, but in oriented nylon, the increase in length is greater along the orientation direction.[47] This shows that the swelling is affected by structure, so the interlamellar and interfibrillar amorphous regions may have different properties and may absorb different amounts of water with different density increases. In this case the X-ray scattering intensity changes that will occur cannot be predicted. Absolute intensity measurements in SANS from unoriented nylon-6 samples swollen with D_2O have been interpreted as showing inhomogeneous swelling of the interlamellar amorphous domains.[48]

Experimental Section

The primary samples were nylon-6 yarn bundles, hot drawn 4.5 times after spinning (roll temperature 175 °C, pin temperature 75 °C). Most X-ray data were collected at the Cornell High Energy Synchrotron Source (CHESS) using the F-1 beamline. An Area Detector Systems Quantum-4 CCD detector with 2304 × 2304 pixels each 82 μm across was used to collect small-angle and wide-angle scattering at the same time. The detector was displaced to put the main beam at one side, far enough from the edge to collect the entire small-angle pattern. With a camera length of 522 mm, a 0.1 mm collimator, and a wavelength of 0.091 nm the first equatorial reflections could be captured on one side, and data extended out to $Q = 20\ \mathrm{nm}^{-1}$ [$Q = 4\pi \sin\theta/\lambda = 2\pi/(d\text{-spacing})$] on the diagonal. The comparatively small (~10 nm) lamellar long spacing in nylon makes it possible to collect an adequate small-angle pattern under these conditions.

Experiments at CHESS used a yarn bundle of fibers. The sequence was as follows: A background pattern, one with no sample present, was first collected as frame 1. A pattern from the original fibers was then recorded as frame 2. This is described as "dry" to distinguish it from later hydrated patterns, although the material was not fully dried, merely at equilibrium in a low-humidity environment. The fibers were then unmounted, soaked in deionized water for 10 min, and remounted, and another pattern was recorded (frame 3). To be quite sure that the sample remained thoroughly wet, the fiber was rewetted in situ using a wick of cotton for another 10 min before taking frame 4. The water source was then removed. Excess water retained in the mounting frame was removed with filter paper, the sample not being touched at all. As soon as this was done, a pattern was recorded, and then more at 26 s intervals for the next 23 min. This gives frames 5−53 while the fiber bundle dried naturally in flowing air (forced-air drying).

Incident beam monitor counts were recorded for each exposure, and a smooth curve drawn through these data was used to normalize incident flux before a normalized air scattering background was subtracted. Many operations were done on smaller sections of the data. These were equatorial and azimuthal sections to study the wide-angle equatorial reflections and a block of 401 × 401 pixels around the main beam to study the small-angle pattern. The detector is made up of four CCD chips in a square array with 400 μm (5 pixel) gaps. Data from these narrow regions were excluded from analysis.

Figure 1 shows a single raw data frame collected from a wet nylon-6 fiber bundle. The gaps in the data appear as white lines in the image. The detector was shifted slightly in a vertical direction

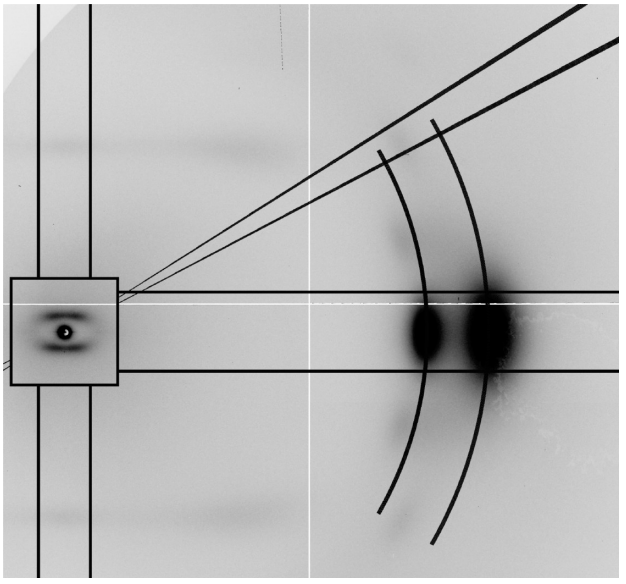

Figure 1. X-ray diffraction data from the nylon-6 fiber bundle. The white lines are the gaps between the CCD detector quadrants. The black lines have been added to show where data were extracted for further analysis.

so that the horizontal gap lies outside the small-angle reflection. In the figure, heavy dark lines have been added to show where data were selected for further analysis. The small box around the origin is the region used to analyze the small-angle pattern. Wide-angle radial intensity distributions were taken in the meridional and equatorial directions within the parallel rails shown. The angular profiles of the two major peaks were measured along the arcs, and the off-axis sector was used to measure the diffraction peak from water at $Q = 16.3$ nm^{-1}.

A second set of experiments used the A-1 beamline at CHESS, a similar detector at 460 mm camera length, a 0.2 mm collimator, and a wavelength of 0.092 13 nm. The samples were a similar fiber bundle wetted with silicone oil (DC704 vacuum pump oil) and a thick (0.7 mm) nylon-6 monofilament. Later, a third experiment of microbeam small-angle scattering[49] was performed at the ID-13 beamline of ESRF with a single fiber of the nylon-6 that was used in the bundle samples. Crossed Fresnel optics produced a microbeam about 400 nm fwhm[50] at a wavelength of 0.0984 nm. This was used to obtain both small-angle scattering patterns and the two inner equatorial wide angle reflections at a camera length of 200 or 300 mm as the fiber was scanned across the beam.[51]

Results

Water Content. X-ray data were used to get a relative measure of the water content of the sample during the experiment. The halo due to water at 20 nm^{-1} [52] is not strong enough to be seen by the eye in Figure 1. However, if a radial section of the diffraction data is taken in a direction where the scattering from nylon is comparatively weak, the water peak (from a wet fiber) is a significant component, and it can be readily separated from scattering due to the nylon. The oblique lines in Figure 1 show the limits of the sector, centered at 30° to the equator, from which data were averaged to determine the water content.

Figure 2 shows the radial intensity in this sector, after background correction. The three data curves in Figure 2 are from the fully wetted sample, frame 6, from the beginning of the drying process, frame 14, and from the sample after most of the water has gone, frame 30. The curves were fitted to three peaks at the fixed positions of the reflection from crystalline nylon, the halo due to amorphous nylon, and the halo due to water.

The curves in the lower part of Figure 2 are the three components of the fit to the intermediate water content curve. The gap in the data near $Q = 11$ nm^{-1} is from the gap between the CCD chips. The width of the water halo was not allowed to change in the curve fitting process, so the height of the outermost peak can be taken as a measure of the amount of water present. The height and width of the sharp peak are constant during the drying process, as they should be if the crystallinity is not much affected.

The height of the water halo, normalized to be unity for the fully wetted sample, is shown as the relative water content in Figure 3 as a function of frame number. This is the exposure number in the experiment as described above. The filled squares at frames 6, 14, and 30 correspond to the curves in Figure 2. They have relative water contents of 1.0, 0.7, and 0.015. In Figure 3 there is a slow loss of about 5% of the water from frame 5 to 12, and then a sharp drop when 90% of the measured water is lost in frames 12−19. Then there is again a slower loss of water, this time with an exponential approach to zero content, detectable until about frame 35. Beyond this point the water content is too low to be measured reliably using the curve fitting of X-ray data.

To estimate the actual water pickup in the X-ray experiment, identical fiber bundles were wetted in the same way and weighed as they dried in air. The result was maximum water content of 45% of the dry fiber weight, falling to 1.5%

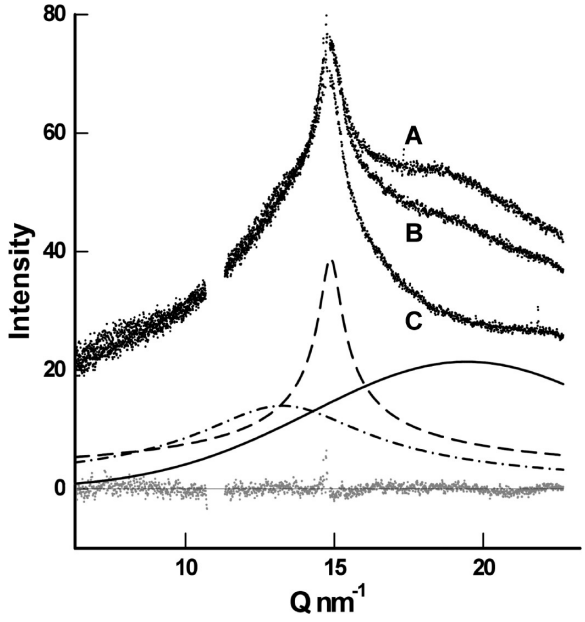

Figure 2. Radial intensity plots at 30° to the equator as used to give relative water content: (A) fully hydrated fibers; (B) during dehydration; (C) at the end of dehydration process. The lower curves are the fitted components for (B) and the residual fitting error.

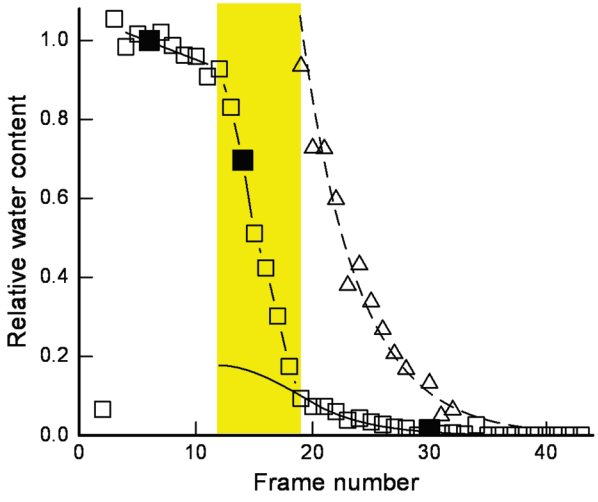

Figure 3. Relative water content set to unity for fully wetted fibers. The triangles are the same data multiplied by 10 to show the exponential fit after frame 20. Solid squares are the examples used in Figure 2. The band between frames 12 and 19 emphasizes the region where most water is lost, for comparison in later figures.

in final equilibrium with dry air (Figure 4). For comparison, the accepted value for absorption of water into these fibers at room temperature is 6−10%.[16,38,47] This confirms what was clear by direct observation, that a lot of water was held between the fibers in a bundle when it was wetted by direct contact with water, instead of by equilibration to saturated vapor. If the total water in the weighed sample is the same as in the X-ray experiment, then about 20% of the water reported in Figure 3 is absorbed into the nylon and 80% is superficial.

There are three disadvantages to the X-ray determination of water content. It is not an absolute measure, it includes surface water in the total, and as it depends on a diffraction halo from liquid water, individual water molecules absorbed and fully dispersed within the polymer may not be properly detected. The advantages are that it is immediate and it refers

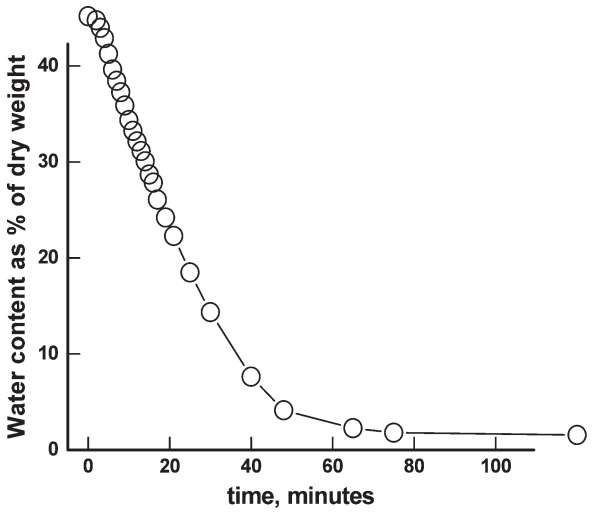

Figure 4. Weight percent water content during air drying, measured by weighing a fiber bundle.

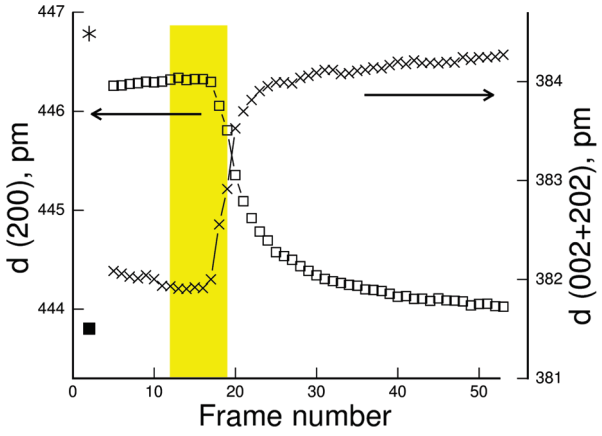

Figure 5. WAX equatorial *d*-spacings as a function of frame number (= time during drying). The asterisk and solid square are the (002) and (200) values for the original fiber.

to the volume of material in the X-ray beam and no other. This explains the main difference between the plots in Figures 3 and 4. The initial small change in water content measured by X-ray occurs when most of the water being lost comes from other parts of the sample. When the drying front passes through the irradiated volume, there is a sudden loss. In contrast, weighing shows the total or average steady loss of water. The weighing data show a slower water loss because the air circulation was stronger in the X-ray experiment.

Wide-Angle Diffraction. The diffraction pattern in Figure 1 shows two strong reflections on the equator. Nylon-6 α-phase is monoclinic, with **b** the fiber axis, so the equatorial reflections are (*h*0*l*). The inner is (200), and the stronger outer reflection is (002) with some (202) contributing. It has previously been shown that on wetting[38] as well as on annealing[53,54] the separation of these two peaks, Δ*d*, increases, and this change is taken to show an increase in crystal perfection. The change on wetting is reversible. Figure 5 shows that on wetting the inner reflection moves in from 0.4439 to 0.4462 nm while the outer moves out from 0.3844 to 0.3819 nm. Almost all of this change is reversed on air drying. Note that rapid change during the drying does not start until frame 17 when the relative water content has fallen to about 0.3, toward the end of the rapid loss of water. This supports the view that the water lost up to this point is largely

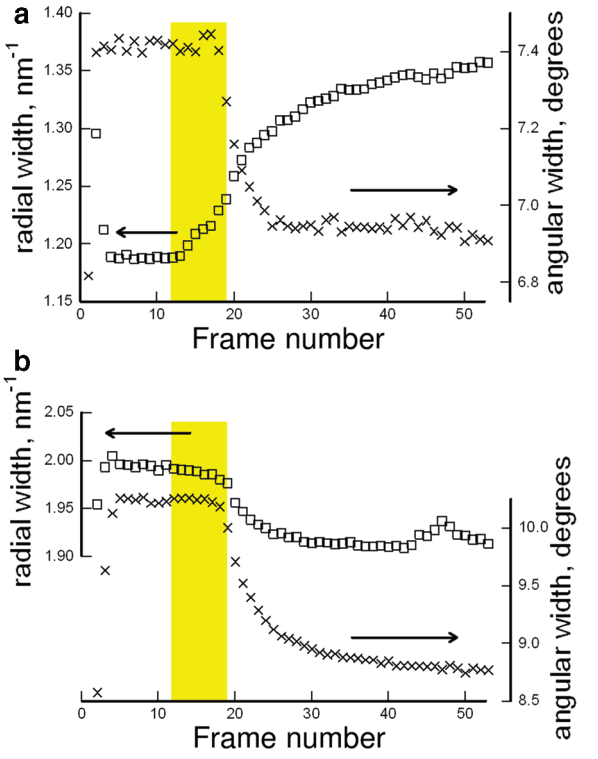

Figure 6. WAX equatorial widths as a function of frame number. (a) is the inner, (200) reflection, and (b) is the outer, (002) + (202) reflection.

superficial. Changes in the WAXD reflections continue to the end of the experiment, when the water content is too small to be measured by the X-ray scattering method.

The WAX peak width in the radial direction is also a measure of crystal size or perfection. The inner (200) peak width is reduced by wetting, and it increases again during drying by about 15% (Figure 6a). If the crystals were perfect and the only cause of broadening the limited crystal size, this would correspond to a reduction in mean size on drying from 5.2 to 4.6 nm. Since the outer peak contains both (002) and (202), its width can be affected by the relative motion of its components, and the observed change in radial width is small and in the opposite direction (Figure 6b).

The peak width in the azimuthal direction is affected both by longitudinal crystal size and perfection and by the range of orientations that the crystals have in the sample. The meridional wide-angle reflection included in the recorded pattern is not significantly changed in spacing or shape by wetting and redrying. Its integral breadth remains at 1.9 nm^{-1} in Q, corresponding to a crystal size in the chain direction of 3.3 nm. The azimuthal width of the equatorial peaks is therefore interpreted as a range of angular orientation, which is also shown in Figure 6. In both reflections there is a reversible increase on wetting. Comparing the curves in Figure 6, the angular width does not begin to change until frames 18 and 19, while the radial width appears to begin to change earlier, at frame 14 for the (200) reflection. The change of misorientation tracks well with the change in *d*-spacing shown in Figure 5.

Small-Angle Scattering. The wide-angle X-ray diffraction patterns in this experiment all look identical to the eye. The changes described above are small; for example *d*-spacings change by only 0.5%. In contrast, the small-angle scattering changes a lot during wetting and drying. Figure 7 shows three small-angle patterns taken from the central region outlined in Figure 1. The images have been corrected for air scatter and normalized to the same incident beam flux.

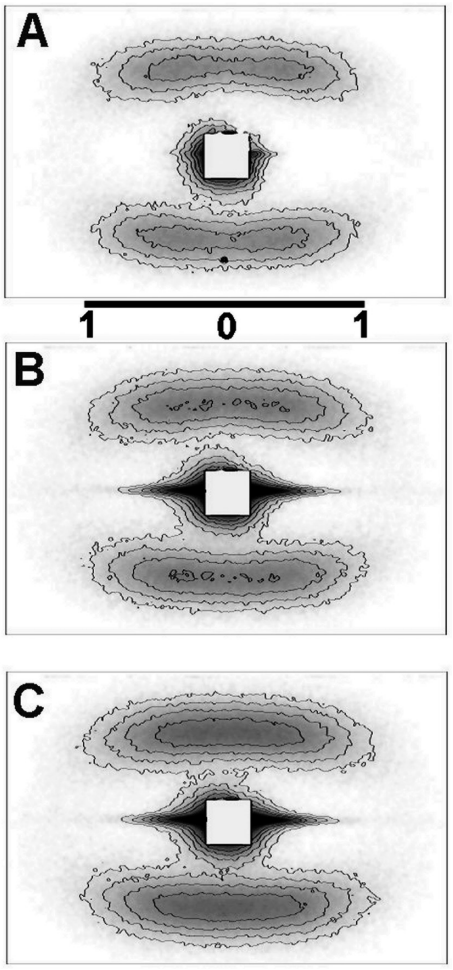

Figure 7. SAXS patterns of nylon-6 fiber bundles Scale bar is Q, in nm^{-1}: (A) frame 6, fully wetted; (B) frame 18, at relative water content 0.2; (C) frame 32, almost fully dried.

Because there is a very wide range of intensities in these patterns, the density in the images indicates the logarithm of the intensity. The contours are at equal logarithmic intervals and are at the same intensity values in every image. Figure 7A is of the fully wetted fiber bundle, frame 6, which is the same pattern used in Figure 1. Figure 7B is from frame 18, relative water content 0.2. Figure 7C is from frame 32, when most changes are over and the sample is close to dry.

In each diffraction pattern there is a central isotropic scatter around the beam stop, and in Figure 7 this is largely blanked out by a square in each image. Figure 7A has an extremely weak equatorial streak and an elliptical four-point pattern from the lamellar structure. In Figure 7B, after 80% of the total water has been lost, a very strong equatorial streak has appeared, but there is little change in the four-point pattern. The streak does not extend further or get stronger in Figure 7C, but there is a more significant change in the lamellar reflection. The pattern now looks like a two-point pattern, with peak intensity on the meridian. Its intensity has increased, and it also appears flatter and less rounded, that is, there has been an increase in ellipticity.

Lamellar Peaks. To measure the characteristics of the small-angle scattering, each data column from the small-angle region parallel to the fiber axis was first fitted to a function with three peaks and a background. Two symmetric Pearson VII peaks corresponded to the lamellar reflection, and a central peak of the same form described the streak. It was found that in dry samples where the equatorial streak

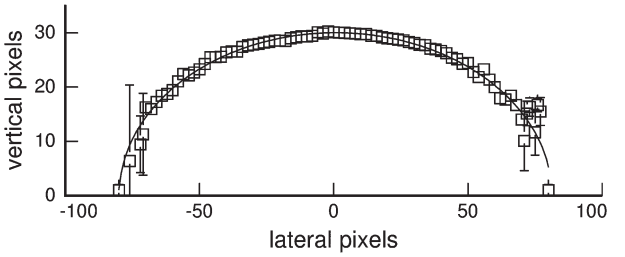

Figure 8. Lamellar peak positions fitted to ellipse. Vertical axis is magnified by 2×.

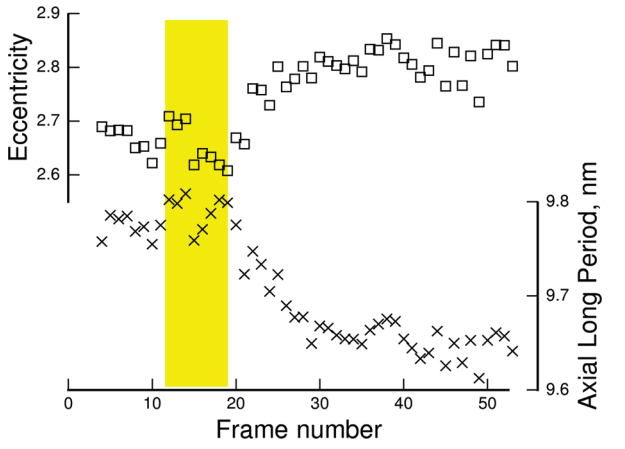

Figure 9. Axial long period and eccentricity of the elliptical fit to the lamellar peaks, both as a function of frame number.

was intense, fitting of the lamellar peaks was distorted by attempts to fit the tails of the strong peak. The central part of the data containing the streak was therefore removed from consideration. The fit was still made with three peaks, but the central peak is now broad and weak, fitting only the tails of the equatorial streak. This does not distort the lamellar reflection fitting so much.

There are many parameters that can be measured from the lamellar reflection. One commonly used is the axial lamellar long period, obtained from the peak position of the reflection on the meridian. This long period changes by a small amount in this experiment, only ~1%, and it is difficult to measure directly. Instead, the fitted functions for each data column were used to give a peak position, peak height, and peak width in the fiber axis direction for the lamellar reflection as a function of Q_x, the distance of the data column from the meridian. Figure 8 shows data for the peak position from frame 6, a "wet" fiber bundle. The positions are an excellent fit to an ellipse,[18,19] even when the peak position approaches the equator (70°−80° from the fiber axis).

With this technique the long period can be determined as the reciprocal of the minor axis of the ellipse. This long period is shown in Figure 9; it changes from 9.78 ± 0.02 nm for the wet fiber bundle to 9.65 ± 0.01 nm for the dry bundle. This reduction of only 1.3 ± 0.3% occurs between frames 18 and 30. Figure 9 also shows how the eccentricity changes from 2.65 ± 0.03 to 2.81 ± 0.03 as the reflection becomes nearer to lying on a layer line on drying. The small changes in these parameters make for noisy results, but the form of the curves in Figure 9 appear to be constant until frames 17−19, followed by an exponential approach to a different value for the rest of the experiment. That is to say, they follow the same pattern as before.

It was remarked earlier that the small-angle pattern of the dry fiber appears to be a two-point pattern, with the peak

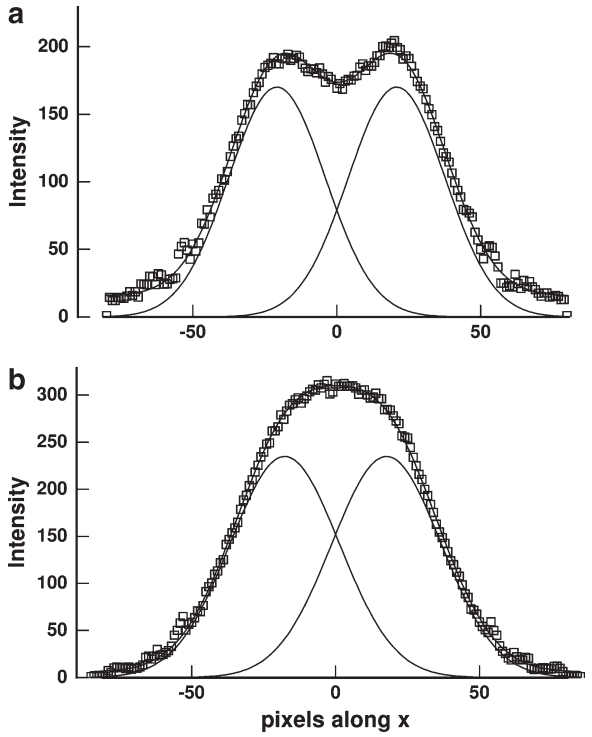

Figure 10. Lamellar peak changes from a four-point pattern, (a) (frame 6), to a two-point pattern which is best fitted by overlapping peaks, (b) (frame 32).

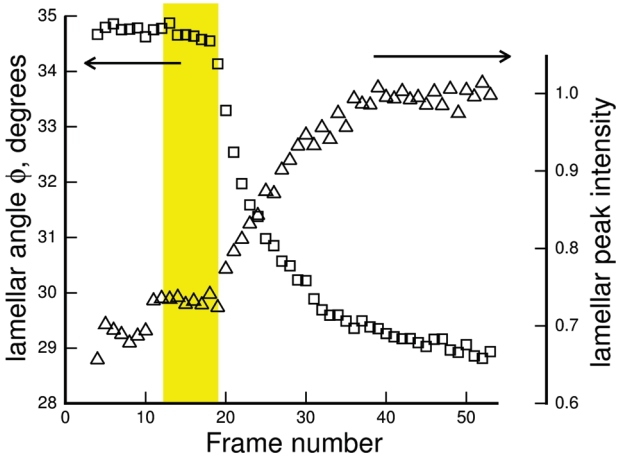

Figure 11. Angular separation of the peaks of the lamellar reflection and intensity of the lamellar peaks, both as a function of frame number.

intensity on the meridian. Plots of the peak height of the reflection in each data column are shown in Figure 10. A fit of these peaks was started with the wet fiber where the pattern clearly has "four points", that is, two separate peaks in each reflection as in Figures 7a and 10a. On continuing with patterns from drier fibers, the best fit contains two separate but now overlapping symmetric peaks; such a fit is shown in Figure 10b. Figure 11 contains a plot of φ, the angle from the meridian of these fitted peaks as a function of frame number. Lateral position (in pixels along x) was transformed to the angle using the known ellipticity of the reflection. The angle φ is almost 35° for the wet fiber bundles. Clearly this parameter follows the same pattern, beginning a rapid change at frame 18 and falling to 29° at the end of the run. Figure 7 shows qualitatively that the intensity of the lamellar reflection increases on drying (an extra contour appears).

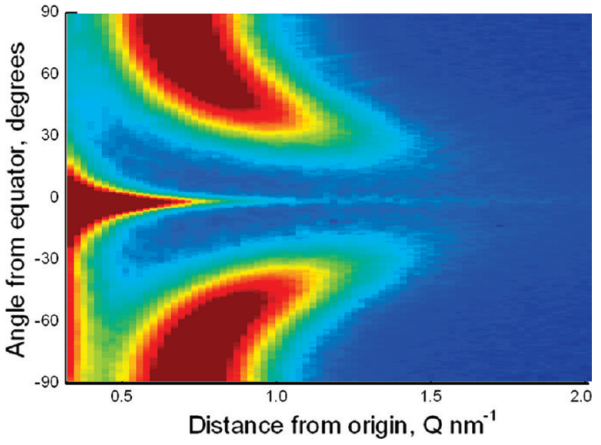

Figure 12. Polar plot of one-half of the small-angle pattern of a dry bundle of nylon-6 fibers.

The integrated intensity is plotted in Figure 11; the increase is nearly 40%, and again the period of rapid change begins at about frame 18.

A different measure of the long period is the average periodicity in the axial direction of all the material contributing to the reflection. To weight the average correctly, allowing for the fact that we are seeing a cross-section of a toroidal reflection in reciprocal space, the intensities are multiplied by the absolute value of the lateral distance from the meridian. The result is a decrease of long period from 10.9 to 10.6 nm, (3%) with rapid change occurring between frames 17 and 26. However, the changes in φ and in ellipticity give more information and are the causes of most of this change in long period; these changes are larger and are acting in opposition.

1-D correlation function analysis[55,56] was used to determine the long period and the fraction of each component in the lamellar stack ("linear crystallinity"). The streak and lamellar intensity overlap, and so do the small-angle and wide-angle signals. This makes background estimation difficult. It was found that reforming the data as a polar or azimuthal (Q, θ) plot helped to separate the equatorial streak from the lamellar reflections. After background was subtracted, the data were retransformed to $x-y$ and projected onto the meridian. It was found that the long period decreased from 10.2 to 9.8 nm on drying, while the linear crystallinity remained constant at 0.64. The long period measured follows the change in the simple average. The linear crystallinity is more sensitive to the choice of background subtraction; different fitting choices increase its value to 0.72, but it still remained a constant during the experiment.

Equatorial Streak. Figure 12 is a polar (Q, θ) plot of one-half of the small-angle region. The equatorial streak is horizontal and at the center. It extends out to $Q = 2$ nm^{-1} and has constant angular width in the outer regions. The tails of the "meridional" lamellar reflections are seen to overlap the streak in the center of the image, on the equator.

For each frame, all slices at constant Q were fitted with a Pearson VII function. In the inner (lower Q) half of frames 14−53 there was more signal, and the streaks were also fitted with a Voigt function. The height of the peak was plotted as a function of Q for each frame, and it was found that in every case for the observable range of Q, the peak height fitted well to a Q^{-4} power law. Examples are shown in Figure 13, where the upper data set is from the pattern in Figure 7B, frame 18. The lower ones are from a wet sample, Figure 7A, frame 6, and from a bundle wetted with silicone oil. The fitted lines have a mean slope of 3.93 ± 0.03.

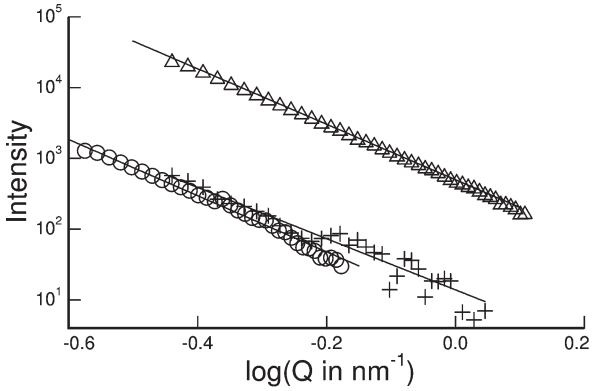

Figure 13. Power-law plots of peak of streak intensity as a function of Q: (△) dry sample, frame 32; (+) water wetted sample, frame 6; (○) oil wetted sample.

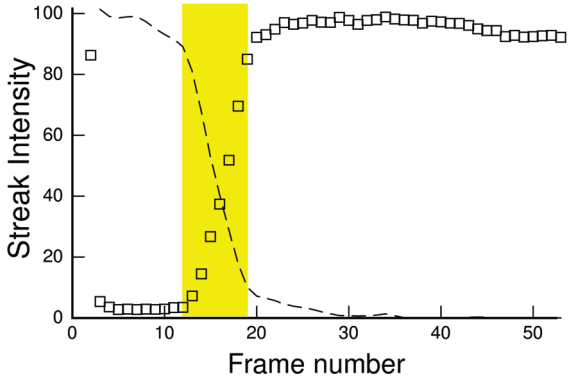

Figure 14. Integrated Intensity of equatorial streak as a function of frame number. The dashed line is the percent total water content, from Figure 3.

From Figure 13, the peak intensity in the fully wetted fibers is about 2% of that in the dried fiber at the same value of Q. Figure 14 is a plot of integrated intensity in the streak as a function of frame number showing the same amount of change. The intensity starts to rise at frame 12, and the change is largely complete by frame 20. There is a small (5%) decline after frame 30 as drying continues. Comparing this to Figure 3, the rapid drop in water content from frame 12 to frame 20 exactly corresponds to the major change in the small-angle equatorial streak intensity; the water content data from Figure 3 is plotted as the dashed line in Figure 14.

Analysis of the width of the streak in the transverse direction as a function of distance from the origin can be used to determine the misorientation of the scattering objects and, by extrapolating to $Q = 0$, their size.[13,22,57,58] Exact extrapolation is possible only if the component distributions are known and of simple form, such as Gaussian, Cauchy, or top hat, not with an empirical function of variable shape like the Pearson VII. Fitting with the Voigt function, which assumes that the broadening is the result of the convolution of a Gaussian with a Cauchy line shape,[59,60] can help resolve this problem.

For each frame with sufficient signal, the equatorial streak is plotted in Q, θ form and its breadth is fitted to a Voigt function at each value of Q. This fitting finds the angular width (integral breadth) of a Gaussian and a Cauchy component. The absolute width (angular width × Q) is plotted as a function of Q for each frame and fitted to a straight line. If a component is only caused by an orientation distribution, the widths will fall on a straight line through the origin and the slope of the line is the integral breadth of the distribution.

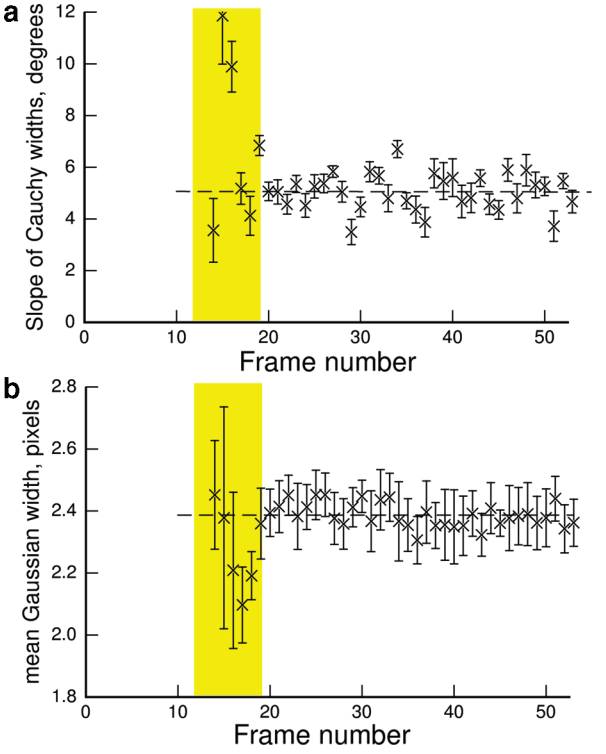

Figure 15. (a) Cauchy streak component width/Q for each frame. (b) Gaussian streak component mean width for each frame.

If it is only caused by a limited size of scattering object, then the widths will be constant and the slope of the straight line will be zero. Typically, it is assumed that the orientation distribution is Gaussian and the size broadening is Cauchy, but in this case the unambiguous experimental result is the other way around.

Figure 15 shows that below frames 17−19 the fitting does not work, but at frame 20 and above the situation is stable as the fiber bundle continues to dry. This "dry bundle" streak contains a peak of Cauchy shape with constant angular width, integral breadth 6 ± 1° equivalent to a fwhm of 4°. (Figure 15 shows 5.1 ± 0.7°, but another fitting scheme gives a constant 6.7°.) The slope determined for the Gaussian component is small but negative. The probable explanation for this is that the size broadening is along z while the orientation broadening is angular. Thus, the (Q, θ) form will "see" off-axis points along an arc which are closer to the origin, and therefore have higher intensity, than the true spread due to size broadening. This will give too broad a result at small radial distances, so the intercept at $Q = 0$ will be too large. Mean data from higher radii where there is less curvature of the arc will be more reliable and are shown in Figure 15 to become constant about frame 20. The Gaussian component is fixed in width at an integral breadth of 2.38 ± 0.06 pixels. Subtracting the nominal beam width, 1.2 pixels, this gives the effective length of the scattering object as 300−500 nm.

The much weaker streaks from the wetter samples cannot be analyzed in such detail. Averaging the signals from frames 5−11 to reduce noise, a fit of width as a function of Q gave a misorientation of integral breadth 6−7.5° and an integral breadth intercept at $Q = 0$ of 3.0 ± 0.5 pixels. These results are identical to the results for the stronger streak, so it appears that only the intensity of the streak is affected by the water content.

Two experiments were conducted to determine if the equatorial scattering depended on the position of the beam

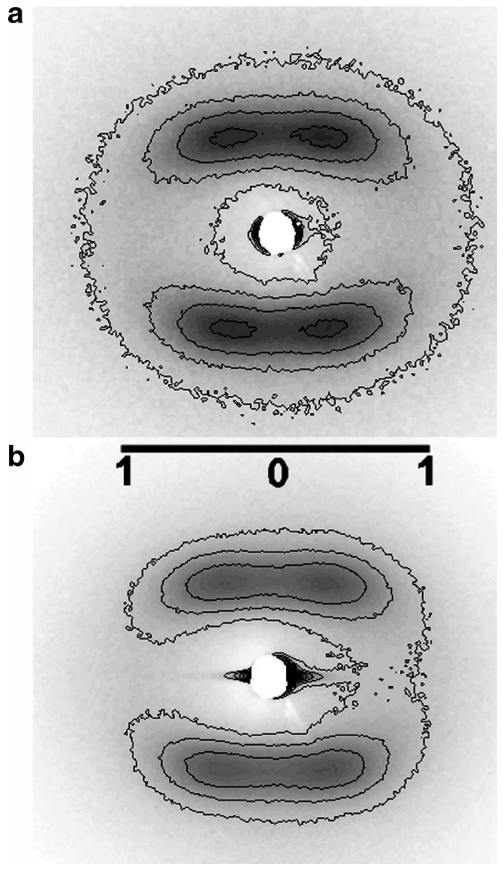

Figure 16. SAXS patterns from a 0.7 mm diameter nylon-6 monofilament. Scale bar is Q, nm^{-1}. (a) The beam is incident on the center of the fiber. There is no equatorial streak. (b). The beam is incident on the fiber edge. There is a weak equatorial streak.

on a fiber. The first used a larger fiber and the results are shown in Figure 16. When a 0.2 mm diameter beam was incident on the center of a 0.7 mm diameter filament, so that the edges were not illuminated, there was no equatorial scattering, but when the edge was illuminated, an equatorial streak appeared. The pattern has internal evidence that the fiber was partially in the beam, as the background is of lower intensity on the left-hand side. This is due to air scatter being absorbed by the sample, and the sample is only present on one side.

The second experiment used the original fiber and a smaller, 0.4 μm, beam. The optics were not optimized for small-angle scattering, so strong streaks appear at $\pm 45°$ due to scattering by the optical focusing elements. Figure 17 shows that it is still clear that the equatorial streak is not present unless the beam intersects the fiber edge. When the beam is central, there is a clear lamellar peak and no streak. The streak in Figure17 is very sharp, but this is to be expected; only a single long diffracting element is illuminated, so there is no orientation distribution. An $x-y$ scan of the sample across the beam showed a detectable streak only within a narrow range of ~750 nm around the position of the edge (Figure 18).

Discussion

The aim of this experiment was to investigate the dynamics of drying; it was hoped that the desorption of water from the amorphous interlamellar regions would be separate in time from the desorption of water from interfibrillar regions, and this distinction would be picked up in the X-ray scattering patterns.

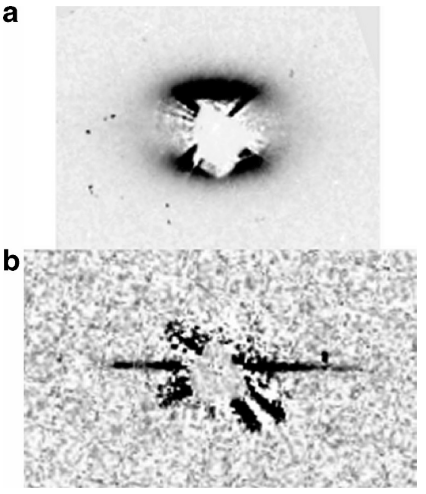

Figure 17. Microbeam SAXS pattern a nylon-6 filament, beam size 0.4 μm. (a) Beam on the fiber center; lamellar peaks but no equatorial streak. (b). Beam on the fiber edge; strong equatorial streak but no lamellar peak.

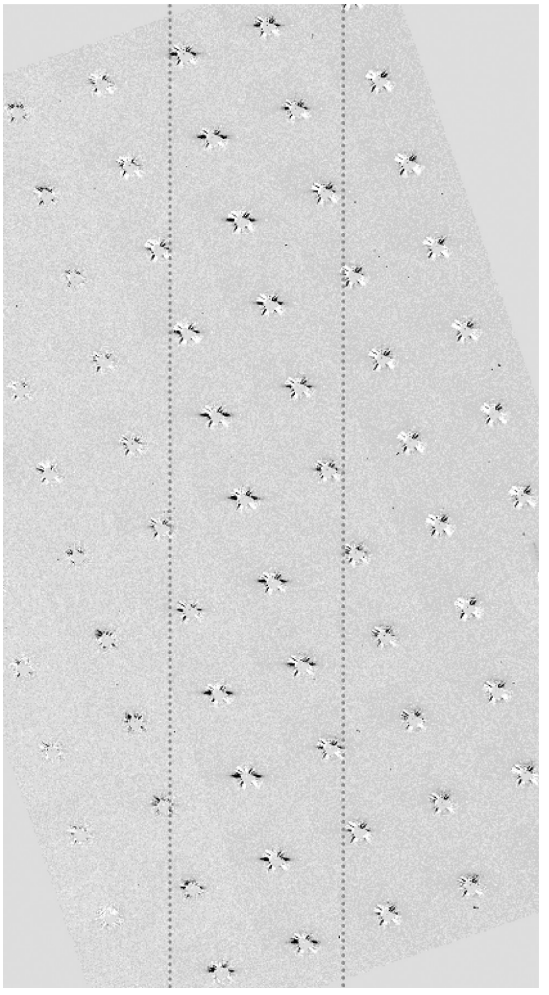

Figure 18. Microfocus SAXS scan of nylon-6 fiber. Patterns were taken every 400 nm. Dotted lines indicate the region, 750 nm wide, where equatorial streaks were seen.

The fiber bundle was not enclosed for the X-ray experiment, so it was wetted with liquid water to make sure that it started off in the fully wetted condition. Capillary action filled the interstices of the fiber bundle with water, so there was initially a significant amount

of superficial water. However, this should not affect internal structure, so its expected effect was simply to delay the process of internal drying.

So much for expectations; what was the result? To summarize all the data presented above, for some time (up to frames 10−12) little happens. Then in the next 4 min (up to frames 18 and 19) 80% of the total water is lost, and the single change in the X-ray results is that the small-angle equatorial streak intensity increases dramatically. After this, the water content falls much more slowly, with an exponential approach to zero. In this time period the equatorial streak does not change, but there is a complex set of changes in the lamellar small-angle reflection and the wide-angle diffraction pattern. The drying sequence shown in Figure 3 has four parts: (1) The initial period of slow loss, frames 5−12. This is easily explained; evaporative loss of superficial water is largely replaced from reservoirs such as the sample holder and the few percent loss may be explained as redistribution of superficial water due to drainage. (2) The period of rapid and linear loss of water, frames 12−19, the shaded region in Figure 3 and subsequent figures. This is apparently due to the boundary transport/evaporation limited loss of superficial water. (3) The later slow loss of water frames 19−35. This is the diffusion-limited loss of absorbed water from within the fibers. (4) In the final period from frame 35 to the end (frame 53) no change in water content can be detected, but slow equilibration with the surroundings is still taking place. During the third period, frames 19−35, when internal water is being lost, the WAXD equatorial peaks change position and width, and the lamellar SAXS four-point pattern changes in position, shape, and intensity. In the last period, frames 35−53, these properties appear to change at a constant (zero) amount of retained water, but the water content really continues to fall, below the detectable level.

In Table 1 the total changes are compared with those seen in static wetting experiments of nylon-6 fibers using SAXS[16] and SANS[39] and with those seen during tensile deformation of nylon-6 fibers in the dry state.[2] The changes in equatorial WAX *d*-spacings agree with previous results,[38] and wetting has an opposite effect to the tensile loading. Axial tension makes the interlamellar amorphous material extend, and Poisson's ratio lateral contraction is constrained by the crystalline lamellar surfaces, which are put into compression. On wetting at no load, the amorphous material swells, and its lateral expansion is constrained by the crystalline lamellar surfaces, which are put into tension. Surface tractions can affect the entire thin lamella, so a slightly different crystal structure is established at a new equilibrium, whether the cause is applied load or internal swelling.

Under axial tension, some tilted lamellae (from the four-point pattern) undergo a discontinuous transformation to zero tilt (two-point pattern),[13] but the net effect is a reduction of mean tilt angle. Wetting makes the tilt angle increase 4°−5° (Figure 10).[16] Since the chain orientation distribution changes by much less than this, 0.4°−1.5°, the tilt occurs primarily by shear (chain slip). Shear to a steeper tilt increases the surface area associated with each chain stem, so this change will reduce the constraints on the amorphous chains at the interface, allowing the amorphous material to expand more.

The wet fibers have a larger long period. The change in mean long period, at 3%, is less than previously seen (9%, for differently prepared fibers[16]) but comparable to the expected fiber length change for a 6−8% uptake of water. On drying, the chains become better oriented on the fiber axis although the fiber is shrinking, so there is clearly no simple affine deformation operating. One explanation is that on wetting, swelling perpendicular to the constraining tilted lamellar surfaces would cause a body rotation of the lamellar stack. If neighbors prevent such a rotation of a relatively long object, then the effect is to move the chain direction away from the fiber axis. This is reversed on drying, causing orientation to improve.

Table 1. Comparison of Current Data with Previous Static Wetting and Tensile Loading Experiments

	previous results		these results	
equatorial WAX	dry fiber tensile deformation[2]		Figures 5 and 6	
	0 MPa	300 MPa	dry	wet
orientation range, deg	7.2	6.2	6.9	7.4
$d(200)$, pm	442	439	443.8	446.3
$d(002 + 202)$, pm	382	384	384.5	381.9
Δd, pm	60	55	59.3	64.4
Δd wetting results from ref 38			60	62.5
SAXS	fiber annealed at 130 °C[16]		Figure 11	
	dry	wet	dry	wet
off-axis angle, deg	31	35	29	34.7
mean long period, nm	9.1	9.9	10.6	10.9
relative intensity	SANS[39]		Figures 11 and 14	
	dry	wet with H_2O	dry	wet
lamellar	< 0.1	0.4	1.0	0.7
equatorial steak	1	3	50	1

The contrast between crystalline and amorphous regions in the dry nylon-6 fibers is low, $\Delta\rho^2 = 0.022$. The observed 30% reduction in intensity for the lamellar reflection on wetting implies that $\Delta\rho^2$ falls to 0.015, but this change only requires a 2% increase in amorphous density which would change the fiber density by less than 1%.

The figures show that there is an exponential approach to the final dried state when the data is expressed as a function of frame number = drying time. As the water content changes in the same way, there is an approximately linear change when expressed as a function of water content. The effects of water absorption in this region are proportional to the amount of water present. The changes generally begin before frame 19, but this is to be expected; the four parts described above for the drying process will overlap. In particular, as superficial water is lost in region 2, frames 12−19, fiber surface becomes exposed to air, and loss of internal water should begin from those regions. Using the observed streak intensity as a measure of exposed surface area (as discussed below), the internal water loss can be extrapolated back to the region of partial surface exposure. This is the solid line in the lower part of the shaded area in Figure 3, which shows that 17% of the detected water is internal in good agreement with the gravimetric estimate of 20%. About half of this water has already been removed by frame 19, so we should expect to see changes due to loss of internal water starting before then.

Looking at Figures 5, 6, and 11, the WAX *d*-spacings and radial width move first as water is lost These are parameters that relate only to the internal organization of the crystals. The WAX angular width and the lamellar SAX orientation start to shift later; they do not change until frame 19, when 50% of the internal water has been lost. Since this is a dynamic experiment, not at equilibrium, it is possible that these slower-moving parameters involving reorientation are retarded by slow flow in the amorphous regions. The lamellar peak requires a sequence of crystalline and amorphous regions, and this lamellar stack is the basis for fibrillar structure. However, none of the parameters or changes described so far relate to fibril structure directly.

Returning now to the equatorial streak, in SAXS from polymer fibers the streak is normally assigned to scattering from voids or from a fibrillar internal structure, where the stacks of lamellar

crystals form long thin objects of higher density than the surrounding matrix. In nylon-6 there is little evidence for voids unless the fibers were heat-treated when wet.[9] Therefore, the streak is usually believed to come from the fibrillar interfaces, and analysis of the streak broadening has been used to derive the fibrillar misorientation and scattering element length.[13,22,58] In contrast, wet-spun fibers such as poly(acrylonitrile) and the carbon fibers derived from them typically have a lot of internal voids, and this is the source of most equatorial SAXS in these materials.[61−64]

In this experiment we find that the intensity of the equatorial streak increases by a factor of 50 as superficial water is removed from the fiber bundle. If the source of the scattering is fibrillar, then water must be removed from the interfibrillar regions at the same time as superficial water *and* the density of these regions must be an excellent match to that of the highly crystalline fibrils when both are wet. The first condition seems unphysical; it implies that fibers in equilibrium with vapor would contain water only in the interlamellar regions. The second condition requires a large increase in the density of interfibrillar material on wetting; this would produce a large increase the fiber density, which is not observed.[16,46]

The relative intensity of scattering from a void that when filled with water, or from any interface that changes from (nylon:air) to (nylon:water), can easily be calculated from the electron densities. The density of this 4.5× drawn fiber is 1.1460 g cm^{-3},[39] and for nylon-6, $C_6H_{11}O$, Z/A is 0.55. This is the same as that for water. The predicted relative intensity of wet:dry is therefore 1:(1.146/0.146)^2 ≃ 1:62. The observed value is 1:50 (Figure 14), in good agreement with the prediction. To find out more about these interfaces, the fiber bundle was wetted with silicone oil. Silicone oil is used as a fiber processing aid and is believed not to be absorbed in nylon.[65] Any change in intensity is then due to the wetting of interfaces that are accessible without diffusion through the solid. The oil used, DC704, is nominally tetraphenyltetramethyltrisiloxane, $(C_6H_5)_4(CH_3)_4Si_3O_2$, Z/A 0.533, density 1.07 g cm^{-3}. This gives a predicted relative intensity wet:dry of 1:100. From Figure 13, the streak intensity from a bundle wetted with this oil is about 70% of that from a bundle wetted with water. This gives an experimental value of the oil-wet:dry ratio of 1:70. Again, this is in good agreement with the prediction; it means that over 99% of the interfaces that are wetted by water are also wetted by silicone oil and are therefore accessible from the outside of the fiber.

It could be that there are accessible voids within the fibers or that silicone oil really does diffuse into nylon-6. The remaining alternative is that the scattering is from the external surface of the fibers. Since external surfaces will only scatter when they are almost parallel to the incident beam, at the edges of the fiber, one way to distinguish these alternatives is to use a beam smaller than the fiber diameter. If there is no equatorial scatter when the beam is incident on the center of the fiber, then the source is at the edges of the fiber. Both the trial with a large diameter filament (Figure 16a) and the trial with a small beam diameter (Figure 17a) show no streak when the beam is incident on the center of the fiber. In principle, this might be caused by voids in the form of thin sheets perpendicular to the fiber radial direction, but then the streak should appear as soon as the beam moves from the center. It does not appear until the beam reaches the edge, as shown in Figure 18. We therefore conclude that the equatorial streak in these fiber bundle samples is scattering by the fiber surfaces.

At longer times, in regions 3 and 4 of the drying process, the streak intensity rises slowly and then falls by about 5%. This could be caused by small reorganizations of the surface or small density changes of the surface. If the surface layers were largely amorphous a 2% fall in amorphous density on drying as predicted from the lamellar reflection intensity change would make the streak intensity drop by 5%.

Surface scattering certainly exists, but the idea that it contributes to or even dominates the small-angle scattering of X-rays or neutrons by polymer fibers is not normally considered. The feeling is that a few interfaces from large objects cannot possibly produce significant intensity, compared to that from the huge interface density from small objects like fibrils. However, Hentschel et al.[27] showed in 1987 that SAXS due to refraction could be seen in metal and glass fibers, which have no other strong SAXS signal, and also in "hard elastic" polypropylene fibers, which have strong void scattering. These authors showed that for refraction from a cylindrical fiber, intensity goes as Q^{-3} (as for Porod scattering). In detail, for a cylinder of radius R, refractive index $n = 1 - \varepsilon$, the refracted intensity/unit length scattered at the small angle 2θ was found, to a good approximation, to be[27]

$$I'(2\theta) = I_0 R\varepsilon^2/\theta^3 \tag{1}$$

I_0 is the incident flux per unit area, so the radius appears in the formula because the sample area illuminated increases with R. For an array of m fibers, length L, the total scattered flux would be $I_0 mRL\varepsilon^2/\theta^3$ and the scattered intensity (flux/unit area) $I_0\varepsilon^2/\theta^3$. Neglecting absorption, ε can be expressed as

$$\varepsilon = \frac{N\lambda^2 r_e}{2\pi} \tag{2}$$

where N is the electron density of the cylinder, λ the wavelength, and r_e the electron scattering length. This gives the scattered intensity/unit area as

$$I(2\theta) = I_0 \frac{N^2\lambda^4 {r_e}^2}{4\pi^2\theta^3} \tag{3}$$

The usual form of the Porod scattering law for a single cylindrical rod, radius R, is[66]

$$I(Q) = I_0 \frac{4\pi\Delta\rho^2 R}{Q^3} \tag{4}$$

$\Delta\rho$ is the electron density difference between rod and surrounding; here let that be the electron density N. Inserting the usually neglected electron scattering length and substituting for Q

$$I(2\theta) = I_0 R \frac{N^2\lambda^3 {r_e}^2}{2\pi^2\theta^3} \tag{5}$$

This is identical in form to the refraction formula, eq 3, and $2R/\lambda$ larger. The difference is because the SAXS formula assumes coherence over the entire diameter of the fiber while refraction assumes complete incoherence. In a more realistic case of partial coherence there is a single answer between the two cases, as there must be, since there is only a single physical interaction that is being described in two ways.[25]

For an order of magnitude estimate of relative intensity, consider 10 nm fibrils in a 10 μm fiber. There will be about a million of them, 1000 to fill the width and 1000 deep, but the interfacial surface will be only 1000× the surface area of the fiber per unit length. On this basis the predicted intensity/unit area from fibrils is 1000× that from fiber refraction. In this case contrast between amorphous material and the fibrils is usually estimated to be 1% that from the fiber surface, so the predicted fibril intensity drops from 1000× to 10× that from refraction. This assumes that the fiber is a smooth cylinder on the scale of the X-ray wavelength, which is unlikely. SEM of these fibers shows that they have long grooves on the surface,[67] and every asperity

can then act as a separate refractive lens. Thus, it is not surprising that refraction and fibril scattering can give comparable intensities that are not distinguishable in the Porod region.

Size determination using the Porod law constant has been used to show that the scattering objects are small. This method is reliable only when the observed scattering levels off at small angles, leaving the Porod regions and approaching the Guinier region of scattering from the whole object. A good recent example of this, where extrapolation to $Q = 0$ is reliable, is in Figure 3 of ref 58. In the present case, a Porod analysis of both "wet" and "dry" streak give a scattering object diameter of 12 nm (assuming that the scattering objects are 60% of the sample). However, the integrated streak intensity from these fibers increases as Q^{-3} for the entire accessible region. Cutting this off to extrapolate to zero intensity at $Q = 0$ arbitrarily reduces the invariant and thus reduces the derived feature size. Previous work[2] has used the lateral extent of the lamellar reflection as another measure of stack width and therefore fibril diameter. This is reasonable if the lamellar reflection extends out along a layer line. Now it is seen to extend along an ellipse; there must be a real distribution of sizes and orientations of scattering objects involved. The spread of the reflection can only give a lower estimate of their mean size.

Conclusions

When a nylon-6 fiber bundle dries in air, the equatorial streak in the SAXS pattern increases in intensity as superficial water evaporates. Later, as absorbed water is lost, there are changes in the lamellar SAXS pattern and in the equatorial WAX reflections. These later changes are approximately proportional to the change in absorbed water content. Separate experiments show that there is no detectable equatorial streak when the X-ray beam does not intersect the edge of a fiber.

The observed changes in the equatorial WAXD reflections and the changes in the lamellar SAXS reflection agree well with previous observations. They can be explained by water being taken up in the interlamellar amorphous regions, causing them to increase in density and in volume. None of the observed changes as absorbed water is lost require the presence of a fibrillar structure or interfibrillar material.

The equatorial streak normally taken to be due to scattering from the fibril interfaces within the fibers is due to scattering from the surfaces of the 30 μm diameter fibers in the bundle. Scattering from these relatively large cylindrical objects is best described as refraction. The current X-ray scattering experiments thus have no evidence supporting the existence of a fibrillar structure and do not see the expected equatorial scattering from fibrils. Absence of equatorial SAX scattering from fibrils is not proof that they do not exist. However, the usual picture of fibrils having significantly higher density than their surroundings and with well-defined and well-oriented boundaries is inconsistent with the data in this case. Either there is no well-defined structure in the expected size range, or the contrast between such a structure and its matrix is low. Perhaps there is interfibrillar material of higher density than normal amorphous material,[68] but it is difficult to reconcile the linear crystallinity of the stack and the fiber density with such a model.

Two things remain to be emphasized. One is that the implication that surface refraction can be important is true for small-angle neutron scattering as well as SAXS. This may explain some otherwise unexpected observations, for example, that the SANS scattering features that give the equatorial steak are highly aligned, even in undrawn fibers.[39] The other is that that we do not mean to imply that surface refraction must be the only or the dominant contributor to equatorial scattering. For example, some nylon-6 fibers have shown peaks superimposed on the equatorial streak of the SAXS patterns,[13] and this small part of the signal cannot come from surface scattering. In other materials fibrillar or void scattering is very well established as the cause of equatorial SAXS. The void content in polyacrylonitrile, for example, can be measured by other physical means,[69] and it gives an intense equatorial scattering.[61−64] The key is that in these cases the small-angle intensity drops below the Porod law predictions at small angles, in some cases showing a clear Guinier region which reflects the size of the whole scattering object, not just the interface. Refraction predicts that the power law intensity continues to ultrasmall angles. However, the simple test for refraction, determining scattering from a sample immersed in a roughly index-matching fluid, has been reported only rarely,[63] and this means that in the majority of cases the contribution of surface refraction is unknown.

Acknowledgment. This work is based upon research conducted at the Cornell High Energy Synchrotron Source (CHESS), which is supported by the National Science Foundation under Award DMR 0225180, using the Macromolecular Diffraction at CHESS (MacCHESS) facility, which is supported by award RR-01646 from the National Institutes of Health, through its National Center for Research Resources. We acknowledge the European Synchrotron Radiation Facility for provision of synchrotron radiation facilities at beamline ID13 and the support and extensive assistance of Drs. Christian Riekel and Richard Davies, without which the experiment at ESRF could not have been performed. The work by NSM was supported by NSF Grant DMR-0735242.

References and Notes

(1) Murthy, N. S.; Minor, H. *Polym. Commun.* **1991**, *32*, 297–300.
(2) Murthy, N. S.; Grubb, D. T. *J. Polym. Sci., Part B: Polym. Phys.* **2002**, *40*, 691–705.
(3) Ginzburg, B. M.; Sultanov, N. *J. Macromol. Sci., Part B: Phys.* **2001**, *40*, 207–230.
(4) Murthy, N. S.; Correale, S. T.; Moore, R. A. F. *J. Appl. Polym. Sci., Appl. Polym. Symp.* **1991**, 185–197.
(5) Murthy, N. S.; Minor, H.; Bednarczyk, C.; Krimm, S. *Macromolecules* **1993**, *26*, 1712–1721.
(6) Katayama, K.; Amano, T.; Nakamura, K. *Kolloid Z. Z. Polym.* **1968**, *226*, 125–134.
(7) Sakaoku, K.; Morosoff, N.; Peterlin, A. *J. Polym. Sci., Polym. Phys. Ed.* **1973**, *11*, 31–42.
(8) Vonk, C. G. In *X-ray Scattering of Synthetic Polymers*; Balta-Calleja, F. J., Vonk, C. G., Eds.; Elsevier: Amsterdam, 1989.
(9) Murthy, N. S.; Reimschuessel, A. C.; Kramer, V. *J. Appl. Polym. Sci.* **1990**, *40*, 249–262.
(10) Matyi, R. J.; Crist, B., Jr. *J. Polym. Sci., Polym. Phys. Ed.* **1978**, *16*, 1329–1354.
(11) Crist, B. *J. Appl. Crystallogr.* **1979**, *12*, 27–33.
(12) Stribeck, N.; Ruland, W. *J. Appl. Crystallogr.* **1978**, *11*, 535–539.
(13) Murthy, N. S.; Bednarczyk, C.; Moore, R. A. F.; Grubb, D. T. *J. Polym. Sci., Part B: Polym. Phys.* **1996**, *34*, 821–835.
(14) Stribeck, N. *ACS Symp. Ser.* **2000**, *739*, 41–56.
(15) Stribeck, N. *J. Appl. Crystallogr.* **2001**, *34*, 496–503.
(16) Baldrian, J. *Polymer* **1991**, *32*, 740–744.
(17) Murthy, N. S. *Text. Res. J.* **1997**, *67*, 511–520.
(18) Murthy, N. S.; Grubb, D. T.; Zero, K. *Macromolecules* **2000**, *33*, 1012–1021.
(19) Murthy, N. S.; Grubb, D. T. *J. Polym. Sci., Part B: Polym. Phys.* **2006**, *44*, 1277–1286.
(20) Statton, W. O. *J. Polym. Sci.* **1962**, *58*, 205–220.
(21) Hoogsteen, W.; Pennings, A. J.; ten Brinke, G. *Colloid Polym. Sci.* **1990**, *268*, 245–255.
(22) Grubb, D. T.; Prasad, K. *Macromolecules* **1992**, *25*, 4575–4582.
(23) Reimschuessel, A. C.; Prevorsek, D. C. *J. Polym. Sci., Polym. Phys. Ed.* **1976**, *14*, 485–498.
(24) Von Nardroff, R. *Phys. Rev.* **1926**, *28*, 240–246.
(25) van de Hulst, H. C. *Light Scattering by Small Particles*; Wiley: New York, 1957.
(26) Davis, T. J. *Acta Crystallogr. A, Found. Crystallogr.* **1994**, *A50*, 686–690.

(27) Hentschel, M. P.; Hosemann, R.; Lange, A.; Uther, B.; Bruckner, R. *Acta Crystallogr. A, Found. Crystallogr.* **1987**, *A43*, 506–513.
(28) Dilmanian, F. A.; Zhong, Z.; Ren, B.; Wu, X. Y.; Chapman, L. D.; Orion, I.; Thomlinson, W. C. *Phys. Med. Biol.* **2000**, *45*, 933–946.
(29) Bravin, A. *J. Phys. D: Appl. Phys.* **2003**, *36*, A24–A29.
(30) Mueller, B. R.; Lange, A.; Harwardt, M.; Hentschel, M. P.; Illerhaus, B.; Goebbels, J.; Bamberg, J.; Heutling, F. *Proc. SPIE Int. Soc. Opt. Eng.* **2005**, *5766*, 1–8.
(31) Starkweather, H. W., Jr.; Moore, G. E.; Hansen, J. E.; Roder, T. M.; Brooks, R. E. *J. Polym. Sci.* **1956**, *21*, 189–204.
(32) Lewis, E. L. V.; Ward, I. M. *J. Macromol. Sci., Part B: Phys.* **1980**, *18*, 1–46.
(33) Murthy, N. S.; Aharoni, S. M.; Szollosi, A. B. *J. Polym. Sci., Polym. Phys. Ed.* **1985**, *23*, 2549–2565.
(34) Zheng, Z.; Nojima, S.; Yamane, T.; Ashida, T. *Polym. J.* **1989**, *21*, 65–76.
(35) Zheng, Z.; Koizumi, H.; Nojima, S.; Ashida, T. *Polym. J.* **1990**, *22*, 31–38.
(36) Somashekar, R.; Annadurai, V. In *Proc. DAE Solid State Phys. Symp.*; Kurukshetra, India, 1998; Vol. *41*, pp 243−244.
(37) Annadurai, V.; Gopalkrishna urs, R.; Somashekar, R. *J. Appl. Crystallogr.* **2000**, *33*, 657–658.
(38) Murthy, N. S.; Stamm, M.; Sibilia, J. P.; Krimm, S. *Macromolecules* **1989**, *22*, 1261–1267.
(39) Murthy, N. S.; Orts, W. J. *J. Polym. Sci., Part B: Polym. Phys.* **1994**, *32*, 2695–2703.
(40) Murthy, N. S.; Akkapeddi, M. K.; Orts, W. J. *Macromolecules* **1998**, *31*, 142–152.
(41) Hutchison, J. L.; Murthy, N. S.; Samulski, E. T. *Macromolecules* **1996**, *29*, 5551–5557.
(42) Loo, L. S.; Cohen, R. E.; Gleason, K. K. *Macromolecules* **1998**, *31*, 8907–8911.
(43) Loo, L. S.; Cohen, R. E.; Gleason, K. K. *Polymer* **2000**, *41*, 7699–7704.
(44) Iwamoto, R.; Murase, H. *J. Polym. Sci., Part B: Polym. Phys.* **2003**, *41*, 1722–1729.
(45) Laredo, E.; Grimau, M.; Sanchez, F.; Bello, A. *Macromolecules* **2003**, *36*, 9840–9850.
(46) Hinrichsen, G. *Colloid Polym. Sci.* **1978**, *256*, 9–14.
(47) Inoue, K.; Hoshino, S. *J. Polym. Sci., Polym. Phys. Ed.* **1977**, *15*, 1363–1378.
(48) Plestil, J.; Baldrian, J.; Ostanevich, Y. M.; Bezzabotnov, V. Y. *J. Polym. Sci., Part B: Polym. Phys.* **1991**, *29*, 509–514.
(49) Riekel, C.; Burghammer, M.; Muller, M. *J. Appl. Crystallogr.* **2000**, *33*, 421–423.
(50) Riekel, C.; Davies, R. J. *Curr. Opin. Colloid Interface Sci.* **2005**, *9*, 396–403.
(51) Zafeiropoulos, N. E.; Davies, R. J.; Roth, S. V.; Burghammer, M.; Schneider, K.; Riekel, C.; Stamm, M. *Macromol. Rapid Commun.* **2005**, *26*, 1547–1551.
(52) Head-Gordon, T.; Hura, G. *Chem. Rev.* **2002**, *102*, 2651–2670.
(53) Park, J. B.; Devries, K. L.; Statton, W. O. *J. Macromol. Sci., Part B: Phys.* **1978**, *15*, 229–256.
(54) Murthy, N. S.; Minor, H.; Latif, R. A. *J. Macromol. Sci., Part B: Phys.* **1987**, *26*, 425–444.
(55) Strobl, G. R.; Schneider, M. *J. Polym. Sci., Polym. Phys. Ed.* **1980**, *18*, 1343–1359.
(56) Goderis, B.; Reynaers, H.; Koch, M. H. I.; Mathot, V. B. F. *J. Polym. Sci., Part B: Polym. Phys.* **1999**, *37*, 1715–1738.
(57) Ruland, W. *J. Polym. Sci., Part C: Polym. Symp.* **1969**, *28*, 143–151.
(58) Astley, O. M.; Donald, A. M. *Biomacromolecules* **2001**, *2*, 672–680.
(59) Langford, J. I. *J. Appl. Crystallogr.* **1978**, *11*, 10–14.
(60) Ida, T. *J. Appl. Crystallogr.* **2008**, *41*, 393–401.
(61) Thuenemann, A. F.; Ruland, W. *Macromolecules* **2000**, *33*, 1848–1852.
(62) Perret, R.; Ruland, W. *J. Appl. Crystallogr.* **1969**, *2*, 209–218.
(63) Gupta, A.; Harrison, I. R.; Lahijani, J. *J. Appl. Crystallogr.* **1994**, *27*, 627–636.
(64) Wang, W.; Sanjeeva Murthy, N.; Chae, H. G.; Kumar, S. *J. Polym. Sci., Part B: Polym. Phys.* **2009**, *47*, 2394–2409.
(65) Buchanan, D. R.; Dumbleton, J. H. *J. Polym. Sci., Part A-2: Polym. Phys.* **1969**, *7*, 113–122.
(66) Porod, G. In *Small Angle X-ray Scattering*; Glatter, O., Kratky, O., Eds.; Academic Press: London, 1982; pp 17−51.
(67) Chang, H. Personal communication, **2000**.
(68) Bukosek, V.; Prevorsek, D. C. *Int. J. Polym. Mater.* **2000**, *47*, 569–592.
(69) Janosi, A.; Grosse, I.; Hermel, G. *Mon. Chem.* **1996**, *127*, 143–158.